Tanzania Journal of Engineering and Technology 2025, **44**(2):386-400
OPEN ACCESS articles distributed under Creative Commons Attribution Licence [CC BY-ND]
Websites: https://ajol.org/tjet; https://tjet.udsm.ac.tz

ISSN 1821-536X (**print**); ISSN 2619-8789 (**electronic**)
https://doi.org/10.52339/tjet.v44i2.1314

Special Issue – 8th International Conference on Mechanical and Industrial Engineering, October 24 – 25, 2024 at The Nelson Mandela African Institute of Science and Technology, Arusha - Tanzania

The Role of Internal Factors on Vehicular Mobility

Aziz Mdimi*, Geoffrey John, Curthbert Mhilu, Hannibal Bwire and Joseph Kihedu

Department of Mechanical and Industrial Engineering, University of Dar es Salaam, P.O Box 35131, Dar es Salaam, Tanzania.

***Corresponding Author's E-mail:** mdimiaziz@gmail.com; ORCID: 0009-0005-7677-535X

ABSTRACT

Vehicle mobility internal factors are influenced by the performance state of the road surface quality, governor, engine, gear train, differential unit and mobility unit. Studies on vehicular mobility models exist for off-road external factors but absent on on-road internal factors. The on-road internal factors model describes the vehicular mobility performance as a function of internal factors. In the current undertaking, results are generated by the determination of mobility performance characteristics with the application of 2nd Order Ordinary Differential Equations and using Laplace operator with MATLAB Software simulation. The effect of road surface against the time taken varies accordingly. At a pedal force of 50 N, a higher road roughness, indicated by an International Roughness Index (IRI) of 2.8 m/km, was observed on a road segment with notable roughness. The time ensued is 96.0 seconds at a tractive force of 4500 N on pedal force of 50 N indicating a longer transacted time and low fuel displacement resulting in lower engine revolution speed. The lowest roughness at a value 2.0 m/km, time taken was 17.5 seconds to cover the distance at a tractive force of 17750 N. The results suggest that the greater road roughness (IRI) may lead to a longer time taken to cover the distance. As a consequence of high IRI a vehicle travels more slowly and impact on overall mobility. Thus, maintenance on the road surface should be done regularly to better road surface quality.

ARTICLE INFO

Submitted: **Apr. 23, 2024**

Revised: **Nov. 26, 2024**

Accepted: **Jan, 30, 2025**

Published: **May, 2025**

Keywords: Internal Factors, Vehicular Mobility, Tractive force, Pedal force, Fuel rack displacement, Road conditions.

INTRODUCTION

Vehicular mobility is influenced by the behaviour of the internal factors. The internal factors sub-system components include governor, engine, gear train, differential unit and mobility unit. Internal factors play a crucial role in vehicular mobility, influencing vehicles operation and performance including aerodynamics, weight and power train efficiency, directly impact its vehicle mobility. For instance lighter materials and efficient engines can enhance fuel economy and performance.

A mechanical governor pump plays a crucial role in regulating the speed and performance of an engine offering significant efficiency and power to ensure sustainable and efficient vehicular mobility (Guzzella and Amstutz , 1998 ; Dhariwal *et al.*, 2000 ; Giri, 2004).

The transmission system composed of differential unit and gear train whereby the gear train adjusts the engines output to provide the appropriate amount of power and torque needed for different driving conditions to operate efficiently at various

speeds (Lin and Xu. 2015). The differential unit allows the wheels to rotate at different speeds, ensuring smooth cornering and distributes the engine's torque which is essential for maintaining traction and control on various road surfaces (Wang, *et al*., 2011; Li *et al.,* 2022).

When the power is differently distributed to the driving wheels a vehicle will demonstrate different fuel consumption, different vehicle mobility and vehicle performance (Vantsevich and Gray, 2009; Andreev *et al*., 2010; Vantsevich, 2015). As evidence, all-wheel drive system has better fuel efficiency and good mobility than a front-wheel drive car with an identical power rating (Attard *et al*., 2011). Vehicle dynamics is a concern of the vehicle's performance in the interaction with its functional surroundings such as energy/fuel efficiency, mobility and traction.

Mobility is a function of the road conditions. The road conditions include the off-road and on-road conditions. The off-road is the condition of road which provides the ability for a vehicle to operate on soft or deformable terrain (Senatore, 2010). The off-road parameters that influence mobility have been extensively studied and pertinent solutions thereof exist. Vehicle mobility performance of off-road conditions is related to the wheel power management. Factors affecting field mobility, tractive efficiency, vehicle mobility and multi-wheel drive vehicles (Grantham *et al*, 2001; Vantsevich and Gray, 2009, Senatore and Sandu, 2011).

The mechanics of vehicle mobility for off-road conditions depend on soft or deformable terrain in which the soil strength, surface shape such as climb, bend and stench come to effect (Serban *et al.*, 2019) The off-road external factors focus on road static properties such as sinkage, slip ratio, slip velocity, whilst the internal factors for the off- road surface focus on dynamic properties such as turning radius, speed, and dynamic load on wheel. The on-road internal factors focus on the vehicle performance characteristics such as engine efficiency, drive train and vehicle speed capability, vehicle behaviour, vehicle body configuration and vehicle operation.

Good road conditions cushion vehicle shock waves, and this cushioning is important for maintaining mobility. In contrast, bad roads result in shock waves that reduce mobility. The good and bad road conditions are functional of either external or internal factors (Serban *et al.*, 2019) and (Mahajan *et al.*, 2006). These depend on two road conditions of off road and on road. The off-road external factors focus on road static properties such as sinkage, slip ratio, slip velocity, whilst the internal factors for the off- road surface focus on dynamic properties such as turning radius, speed, and dynamic load wheel. The external factors of the on-road conditions refer to road conditions which interact with tyres, vehicular motion, traffic flow, traffic control mechanism road obstacles.

On the other hand on-road conditions refer to the interaction of the vehicle tyre and the road surface making the grip surface, the vehicle speed, engine and mechanical characteristics of the vehicle. Information in record has been studied mobility model known as Mobile Ad Hoc Networks (MANETs) and the results are satisfactory in so far as mobility is considered (Mahajan *et al.*, 2006).

Rolling resistance is produced by increase in traffic flow load and high weight of the tyre (Botshekan, *et al.,* 2019). Rolling resistance causes the wheel to deform and lose energy, which makes it harder for the wheel to keep rolling smoothly Beuving *et al.* (2004), energy dissipation in the suspension system of the vehicles (Sandberg *et al*., 2011; Louhghalam *et al*., 2015;).

Rolling resistance is a contributor to road wheel interaction and affects vehicle operation cost (Flintsch *et al*.,2003 ; Chatti and Zaabar 2012). The development of a mechanistic model for rolling resistance-induced dissipation has yielded results that

identify the key parameters driving fuel consumption and related greenhouse gas emission caused by surface roughness Louhghalam *et al*.,(2015). LevuLytė *et al* (2014) used mathematical model of road-pavement-vehicle interaction and investigated the vibrations exited on the body of a vehicle driving on a rough road. It has been found that when a vehicle is moving at higher speed, its response to pavement rolling resistance is weaker due to the reduction in tractive force caused by the interaction between the tyre and the road surface.

This paper focuses on a model to quantify the relationship between vehicle internal factors such as engine efficiency, drive train, vehicle speed, acceleration and quality road surface such as road obstacles, road surface conditions and interdependent vehicular motion and quality road surface since it affect the time taken to cover the distance. In contrast to empirical approaches, the originality of the approach herein developed relies on inter relationship between road surface factors and vehicle internal factors with results from Laplace transfer function system to analyze the effect of road surface quality on vehicle mobility and its impact on travel time.

METHODS AND MATERIALS

Mathematical Modelling Approach

The approach deploys both analytical and numerical methods using Ordinary Differential Equations (ODE) to develop sub-system internal factors of a vehicle based on deriving. An Ordinary Differential Equation for each of the system components was considered and numerical integration method was adopted to solve transfer function equations using MATLAB. The considered system constitutes of speed governor, engine (prime mover), as well as gear train unit and a differential unit for torque distribution to wheels (mobility performance unit). The resulting conceptual model involve integrating findings from a determination of mathematical expressions for each individual system components of the model developed which affect mobility internal factors such as Governor, Engine, Gear train, Differential unit and Mobility performance unit based on Vehicular mobility performance characteristics is presented in form of block diagram given in Figure 1.

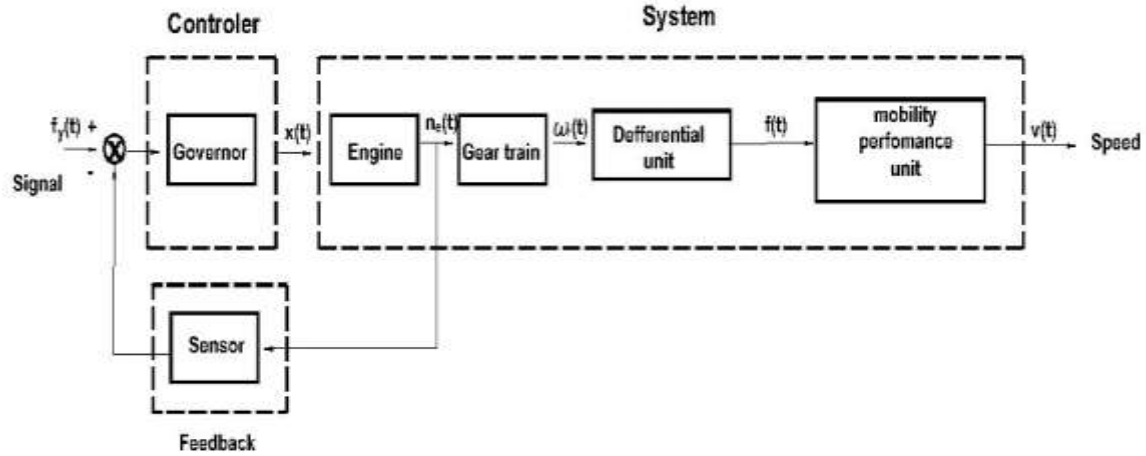

Figure 1: Conceptual block diagram of vehicular mobility characteristics model

where, $\boldsymbol{f_y(t)}$ is the force applied on to vehicle accelerator pedal (N), $\boldsymbol{x(t)}$ is the governor fuel rack displacement (mm), $\boldsymbol{n_e(t)}$ is the engine speed (rpm), $\boldsymbol{\omega_1(t)}$ is the angular speed of the primary shaft of gear train (rad/s), $\boldsymbol{f(t)}$ is the engine's tractive force (N) and $\boldsymbol{v(t)}$ is the vehicle mobility speed (m/s).

Sub-models Formulation

In order to assess the resulting model, each

of the sub-system was assessed to be used for studying the characteristics.

Model of accelerator pedal travel and force of the human leg

The model input is the driver's leg force $\mathbf{f_y(t)}$on the accelerator pedal and applying the spring and force for simulating method. The force applied to the accelerator pedal $\mathbf{f_y(t)}$ and the resulting pedal displacement $\mathbf{y(t)}$ can be obtained from the following expression;

$$\mathbf{f_y(t)} = \mathbf{k_s y(t)} \quad (1.0)$$

where, $\mathbf{f_y(t)}$ is the force applied on accelerator pedal (N), $\mathbf{y(t)}$ is the accelerator pedal displacement (mm) and $\mathbf{k_s}$ is the spring constant (or constant rate in N/m).

Sub-system governor model

The governor controls the speed of the engine by measuring angular speed of an engine ($\boldsymbol{\omega_e}$) in (rad/s) and responding to speed variations due to operating conditions (Dhariwal *et al.*, 2000). To predict the effects of the speed governor on the vehicle mobility, use of the position of the flyweight mass, fuel rack displacement, damping coefficient and spring stiffness of k, is given by expression (Bosch, 2022). To model the corresponding governor rack displacement x(t) in response to the accelerator pedal force $\mathbf{f_y(t)}$, use has been made of the engine governor modelled in the form of a spring-mass damper system to be equal to zero as shown in Equation (2)

$$\sum \boldsymbol{F(t)} = \boldsymbol{m\frac{d^2x(t)}{dt^2}}$$

where, the sum of the forces acting in the system *F(t)* is called tractive forces illustrated the forces on the diagram below, Figure 2

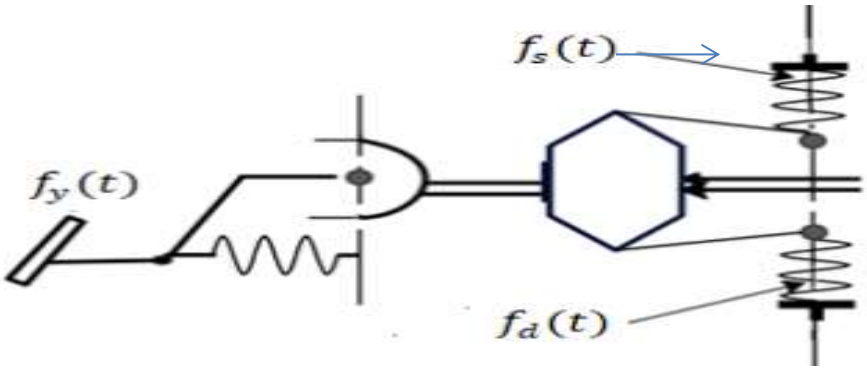

Figure 2: Schematic diagram of an accelerator pedal spring-mass damper system

Note: Arrow show direction of forces $f_y(t)$, $f_s(t)$ and $f_d(t)$

To model the spring – mass damper system use is made of the equilibrium condition taking into account of all forces acting in the system to be equal to zero

The sum of the forces acting in the system is expressed as

$$\sum \boldsymbol{F(t)} = \boldsymbol{f_y(t) - f_s(t) - f_d(t)}$$

The force in accordance to Newton's 2nd law of motion is proportional to rate of change of momentum can be expressed as follows;

$$\sum F(t) = m\frac{d^2x(t)}{dt^2} \quad (3)$$

After substitution we obtain the following equation to be used to model the governor. The model the governor is presented in Equation (4) as;

$$\boldsymbol{m\frac{d^2x(t)}{dt^2} = f_y(t) - f_s(t) - f_d(t)} \quad (4)$$

where, m is the mass of governor flyweight, in (kg), $\frac{d^2x(t)}{dt^2}$ is the acceleration of the body in m/s^2, $f_y(t)$ is the force applied on to vehicle accelerator pedal (N), $f_s(t)$ is the force in (N) exerted by the spring, $f_d(t)$ is the force in (N) exerted by the damper

To obtain the mathematical equation describing the relationship between a spring and displacement it is assumed that the force is proportional to fuel rack displacement $x(t)$ in (mm) and is expressed as:

$$f_s(t) = kx(t) \quad (5)$$

where, k is proportionality constant called spring stiffness.

Assuming the force exerted by the damper to be proportional to the rate of displacement. Hence;

$$f_d(t) = c\frac{dx(t)}{dt} \quad (6)$$

where, c is a proportionality constant called viscous damping constant, whose value depends on the type of cylinder fluid used.

Substituting Equation (5) and (6), Equation (7) is obtained as:

$$m\frac{d^2x(t)}{dt^2} = f_y(t) - kx(t) - c\frac{dx(t)}{dt} \quad (7)$$

This can be re-arranged into the following form:

$$m\frac{d^2x(t)}{dt^2} + c\frac{dx(t)}{dt} + kx(t) = f_y(t) \quad (8)$$

Equation 8 can be re-arranged as:

$$\frac{d^2x(t)}{dt^2} + \frac{c}{m}\frac{dx(t)}{dt} + \frac{k}{m}x(t) = \frac{1}{m}f_y(t)$$

Putting $\frac{c}{m}$ = a; $\frac{k}{m}$ = b; $\frac{1}{m}$ = d are the calculated governor parameters

Taking the Laplace transform of the system under zero conditions Equation 9 becomes:

$$s^2X(s) + asX(s) + bX(s) = dF_y(s) \quad (9)$$

The resulting transfer function is presented in Equation (10).

$$\boldsymbol{G(s) = \frac{X(s)}{F_y(s)} = \frac{d}{s^2 + as + b}} \quad (10)$$

where, $\boldsymbol{G(s)}$ is Transfer function of the governor, $\boldsymbol{X(s)}$ is the fuel rack displacement in mm, and $\boldsymbol{F_y(s)}$ is the force applied on to vehicle accelerator pedal (N).

The resulting block diagram for the governor is represented as in Figure 3.

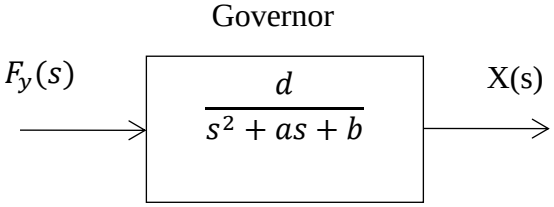

Figure 3: Block diagram of the Sub-system governor

Sub-system engine model

In this study the relationship between fuel rack displacement and engine speed, is determined by making use of a mathematical equation developed by Dhariwal *et al.*, (2000) presented in the form of Equation (11).

$$\boldsymbol{\tau_e\frac{dn_e(t)}{dt} + K_e n_e(t) = x(t)}$$

where, $\boldsymbol{\tau_e}$ is the time constant of the engine in (sec), $\boldsymbol{n_e}$ is the engine speed obtained from the sensor of revolution per minutes (rpm), $\boldsymbol{K_e}$ is the dimensionless coefficient

of self –regulation of the engine.
The resulting transfer function is obtained as shown in Equation (12).

$$\boldsymbol{G_e(s) = \frac{N_e(s)}{X\,(s)} = \frac{1}{\tau_e S + K_e}} \quad (12)$$

where, $\boldsymbol{\tau_e}$ is the time constant of the engine, $\boldsymbol{K_e}$ is the dimensionless coefficient of self-regulation of the engin. The corresponding block diagram is shown in Figure 4

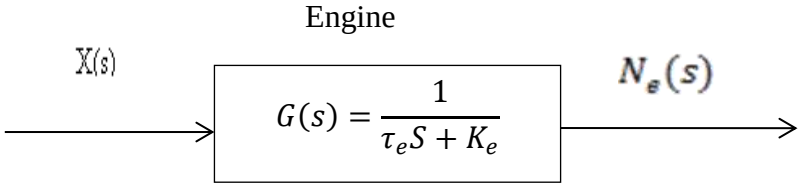

Figure 4: Block Diagram of the Sub-system engine model

Sub-system Gear train model
The relationship between engine speed $\boldsymbol{n_e(t)}$,and the resulting angular speed $\boldsymbol{\omega_1(t)}$ of the output secondary shaft can be expressed with relation to input engine speed as shown in Equation (13).
The gear ratio was taken to be 1:1 as direct drive

$$\boldsymbol{\omega_1(t) = \frac{2\pi n_e(t)}{60} = \frac{\pi n_e(t)}{30}} \quad (13)$$

where, $\boldsymbol{\tau_n = \frac{30}{\pi}}$ a constant, $\boldsymbol{\omega_1}$ is the gear train
The corresponding transfer function is presented in Equation (14)**.**
From Laplace transformation;

$$N_e\,(s) = \tau_n \omega_1(s) \quad (14)$$

The corresponding transfer function is

$$G_s(s) = \frac{\omega_1(s)}{N_e(s)} = \frac{1}{\tau_n} \quad (15)$$

Hence, the resulting block diagram is;

$$\omega_1\,(t) = \frac{1}{\tau_n}\, n_e(t) \quad (16)$$

$$\boldsymbol{G(s) = \frac{\omega_1(s)}{N_e(s)} = \frac{1}{\tau_n}} \quad (17)$$

where, $\boldsymbol{G(s)}$ is the transfer function of gear train, $\boldsymbol{\omega_1(s)}$ is the angular speed of gear train, $\boldsymbol{N_e(s)}$ is the engine speed in terms of transfer functionHence, the resulting block diagram is given in Figure 5

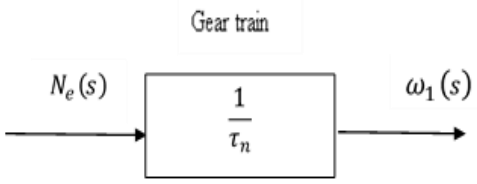

Figure 5: Block diagram of the Sub-system Gear train model

Sub-system Differential unit model
The speed ratio relationship with tractive effort transmitted through the gear train and differential unit is obtained by making use of a mathematical equation expressed in form of gear ratio as shown in Equation (18a).

$$\boldsymbol{\tau_r = \frac{\omega_2(t)}{\omega_1(t)}}$$

From Laplace transform obtained in Equation (18b).

$$\boldsymbol{\omega_2 = \tau_r\, \omega_1(t)}$$

where, $\boldsymbol{\tau_r}$ represents Differential unit gear ratio 4:1, hence, $\boldsymbol{\tau_r}$ = 0.25, angular speed of differential unit ($\boldsymbol{\omega_2}$) in (rad/sec), angular speed of gear train ($\boldsymbol{\omega_1}$) in (rad/sec).

The corresponding transfer function is $\boldsymbol{G(s)}$ as shown in Equation (19).

$$\boldsymbol{G(s) = \frac{\omega_2(s)}{\omega_1(s)} = \tau_r}$$

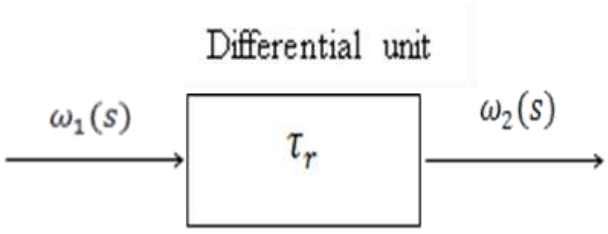

Figure 6: Block Diagram of the Sub-system Differential unit model

Sub-system Tractive Force model

The expected vehicular translational speed can be expressed by making use of the momentum equation put into the form of Equation (20a).

$$\boldsymbol{\beta F_t = M_v \frac{dv(t)}{dt}} \quad (20a)$$

where, $\boldsymbol{\beta}$ is number of driving wheels. For the purpose of this study $\boldsymbol{\beta}$ = 2 wheels.

The vehicular translational motion as a function of angular speed and the wheel radius is;

$$v(t) = R_w\omega_2(t) \quad (21)$$

Where; wheel radius R_w in (m) and differential angular speed $\omega_2(t)$ in (rad/s) remain constant and;

$$\frac{dv(t)}{dt} = \frac{d(\omega_2 R_w)}{dt} = R_w\omega_2(t)$$

Then the resulting expression for the tractive force becomes;

$$F_t(t) = \frac{R_w}{\beta}\omega_2(t) \quad (22)$$

From differential equation above, the corresponding Laplace transform becomes;

$$F_t(s) = \frac{R_w}{\beta}\omega_2(s) \quad (23)$$

The block diagram representing the transfer relationship between the differential angular speed and the resulting tractive force is as given in Figure 7

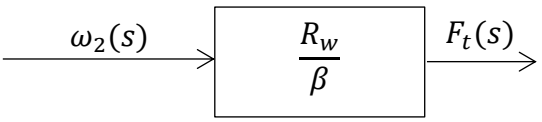

Figure 7: Block Diagram of the Sub-system Tractive Force model

Determination of the overall transfer function for vehicle. The overall transfer function obtained emulating speed governor settings and the resulting tractive effort realised is presented in Figure 8 Vehicle system.

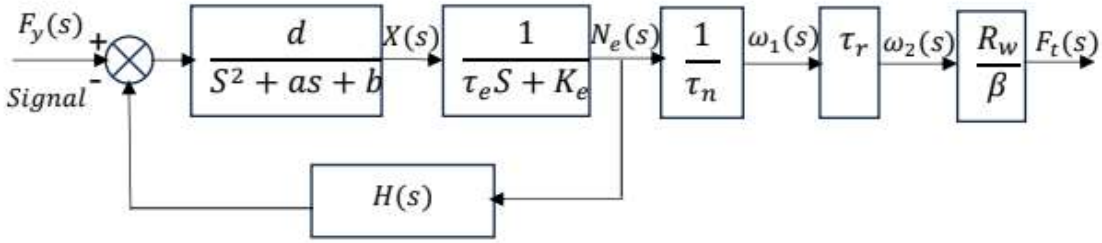

Figure 8: The Overall Transfer Function of Test Vehicle

where, $\boldsymbol{F_y(s)}$ is the force applied on to vehicle accelerator pedal (N), $\boldsymbol{X(s)}$ is the governor fuel rack displacement (mm), $\boldsymbol{N_e(s)}$ is the engine speed (rpm), $\boldsymbol{\omega_1}$(s) is the angular speed of gear train (rad/s) is the input to the differential unit, $\boldsymbol{\omega_2}$(s) is the angular speed of differential unit rad/s) is the output of the differential unit, $\boldsymbol{F_t}$ (s) is the engine's traction force (N).

In this study the discussion of vehicle fundamentals will be restricted to vehicular mobility performance internal factors affecting mobility through speed. The speed is affected by movement behavior of a vehicle along a given direction is completely determined by all forces acting on a vehicle tyre.

The tractive force (F_t) in the contact area between the tyres of the driven wheels and road surface condition moves the vehicle forward. It is produced by the engine torque transferred through the transmission system and final drive to the driven wheels. When the vehicle is moving, there is resistance causing the wheel to stop its movement. The resistance is usually a result of forces due to tyre rolling resistance (F_r), aerodynamic drag (F_d) and uphill resistance (gradient force) F_g . For the purpose of this study it is assumed that the surface is horizontal and all forces acting during the vehicular motion to be equal to its rate of motion change of its momentum. Hence the dynamic equation used to model the vehicle can be expressed in the following form:

$$M_v \frac{d^2v(t)}{dt} = \beta F_t(t) - F_d(t) - F_r(t) \quad (24)$$

where, β- is the number of driving wheels, M_v – is the vehicle mass (kg), and $v(t)$ is the vehicle mobility speed (m/s). It is assume that inertia of the rotating mass is negligible.

Equation (24) suggests that assuming linear motion, vehicle acceleration of vehicle with mas M_v is equal to the difference between the total tractive force available at the tyre-road contact and the aerodynamic drag on the vehicle plus friction resistance. Re-arranging this Equation (24) yields;

$$M_v \frac{d^2v(t)}{dt} + F_d(t) = \beta F_t(t) - F_r(t) \quad (25)$$

In Equation (25), the aerodynamic force is expressed as:

$$F_d(t) = \frac{1}{2}(C_d\rho_{air})A_v v^2 \quad (26)$$

where, ρ_{air} is the air density in kg/m^3, C_d is the coefficient of aerodynamic resistance (dimensionless), A_v is the frontal area of the vehicle in m^2 and v is the speed of vehicle in m/s;

but $v = \omega R_w$

where, v is the speed of vehicle in m/s, ω is the angular speed of the wheel vehicle in rad/s and R_w is the radius of the vehicle wheel in m.

$$F_d(t) = \frac{1}{2}(C_d\rho_{air})A_v(R_w\omega_2)v(t) \quad (27)$$

After some re-arrangements, we obtain:

$$F_d(t) = K_o A_v (R_w \omega_2) v(t) \quad (28)$$

where, $K_o = \left(\frac{C_d \rho_{air}}{2}\right)$= constant

It is also assumed that the expected tyre rolling friction (resistance) (F_r) can be modelled using the expression for given as;

$$F_r = IRI(M_v)\frac{dv(t)}{dt} \quad (29)$$

where, the constant (IRI) represents the International Roughness Index which is a function of road conditions.

Substituting Equations 28 and 29 into Equation 25 we obtain;

$$M_v \frac{d^2v(t)}{dt} = \beta F_t - K_o A_v (R_w \omega_2) v(t) - IRI(M_v)\frac{dv(t)}{dt} \quad (30)$$

After some re-arrangements the equation reduces to:

$$\frac{d^2v(t)}{dt} + IRI\frac{dv(t)}{dt} + \frac{K_o}{M_v} A_v (R_w \omega_2) \mathrm{v(t)} = \frac{\beta}{M_v} F_t(t) \quad (31)$$

Taking Laplace transform of Equation 31 we have;

$$s^2 V(s) + (IRI)s\mathrm{V(s)} + \frac{K_o}{M_v} A_v (R_w \omega_2) \mathrm{V(s)} = \frac{\beta}{M_v} F_t(s)$$

In order to evaluate the vehicular mobility based on the surface conditions use is made of the derived model expressed in the form of a transfer function given in the form;

$$G(s) = \frac{V(s)}{F_t(s)} = \frac{\frac{\beta}{M_v}}{s^2 + \boldsymbol{IRI}s + \frac{K_o}{M_v} A_v (R_w \omega_2)} \quad (32)$$

where, $\boldsymbol{G(s)}$ is the transfer function of mobility , K_O = aerodynamic drag, $\boldsymbol{\beta}$- is the number of driving wheels , $\boldsymbol{\rho_a}$ is the air density in $\boldsymbol{kg/m^3}$, $\boldsymbol{C_d}$ is the coefficient of aerodynamic resistance (dimensionless), $\boldsymbol{A_v}$ is the frontal area of the vehicle in $\boldsymbol{m^2}$ and $\boldsymbol{v}$ is the speed of vehicle in $\boldsymbol{m/s}$, $\boldsymbol{R_w}$ is the radius of the vehicle wheel in $\boldsymbol{m}$, the constant (IRI) represents the International Roughness Index which is a function of road conditions, $\boldsymbol{\omega_2}$(s) is the angular speed of differential unit (rad/s), $\boldsymbol{F_t}$ (s) is the engine's traction force (N).

The block diagram used to model vehicular mobility is presented in Figure 9.

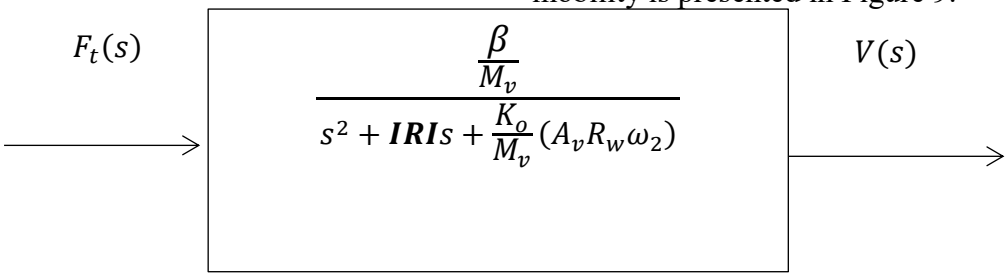

Figure 9: Block diagram of the Mobility Performance Unit

RESULTS AND DISCUSSION

Road rolling resistance analysis data is associated with the recommended minimum International Standard Organization (ISO) values of less than 3.0 m/km. Consider measured value of 2.0 and 2.8 IRI from Table 1 is within the ISO minimum value signifies a normal road surface which not affect the average degree of mobility in terms of speed, energy dissipation in the suspension system of the vehicles and by severe increase in traffic

load and high air pressure of the tyre (Lei *et al.*, 2017 ; Botshekan *et al.*,2019) but extremely smooth roads can also lead to reduced tyre road friction, affecting braking performance and safety. Poor mobility result into excess fuel consumption (Botshekan *et al*., 2019); and (Louhghalam *et al*., 2015). If the actual IRI is less than the ISO minimum, it means the road surface is smoother than the standard. Smoother roads generally offer better speed, ride comfort, reduce vehicle wear and improved fuel efficiency.

Model performance Analysis

Analysis is made on simulation data obtained by running a MATLAB program with roughness (IRI) values in [m/km], given in Table 1. The measured values obtained from the road segment 2.0 m/km as minimum and 2.8 m/km is maximum these are the input values used for simulating data. The 3.0 m/km is the standard value.

Table 1: Input pedal force corresponding Tractive force with Roughness values
Means stipulated standard value of roughness < 3.0 m/km) was used for analysing.

S/N	Pedal force $\boldsymbol{f_y(t)}$ [N]	Tractive force [N]	Segments roughness IRI m/km (Measured)		Roughness IRI m/km: Stipulated standard value < 3.0
1	50	4500	2.8	2.0 *	3.0
2	100	8800			
3	150	13100			
4	200	17750			

Figure 10 shows simulation responses of the measured road segment on a surface of roughness of IRI = 2.8 m/km along a segment length of 2500 m at a speed of 47 m/s. This data suggests a relationship between the tractive force applied and the time taken to cover the distance. As the tractive force increases, the time taken decreases. Higher forces cause greater accelerations, leading to shorter times to reach a destination. The time does not decrease linearly as the force increases. Instead, the reduction in time appears to slow as the tractive force becomes very large, indicating diminishing returns.

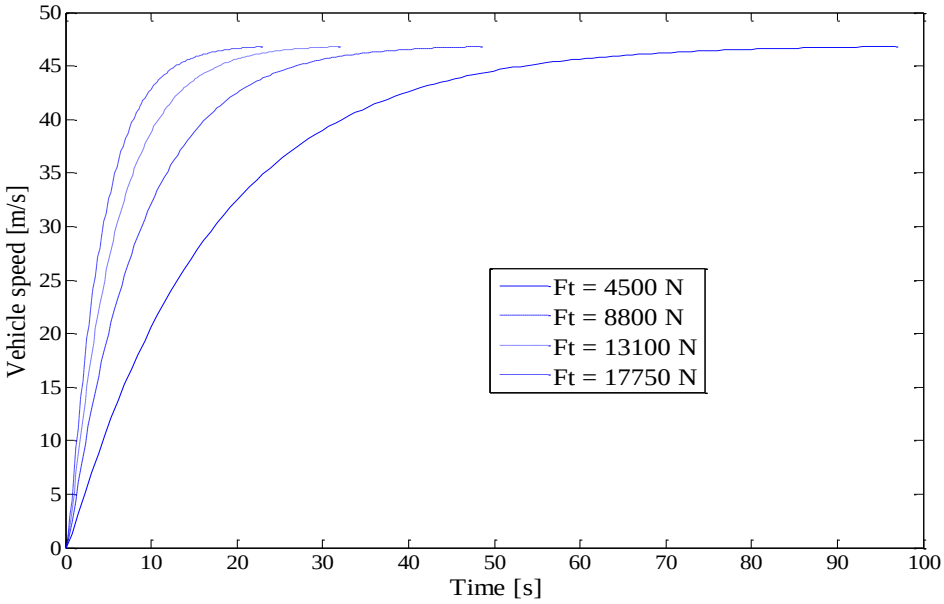

Figure 10: Vehicular Mobility Results of the Measured Road Segment at IRI 2.8 m/k

Figure 11 .show case for a road segment which has a length of 1000 m. In considering simulation response, vehicle was run at a speed of 47 m/s on road roughness with value 2.0 m/km. The time taken to cover the distance at a tractive force of 4500 N was 67.5 seconds. Similarly, the time taken to cover the tractive forces of 8800 N, 13100 N and 17750 N was 33.0 seconds, 32.0 seconds and 17.5 seconds respectively.

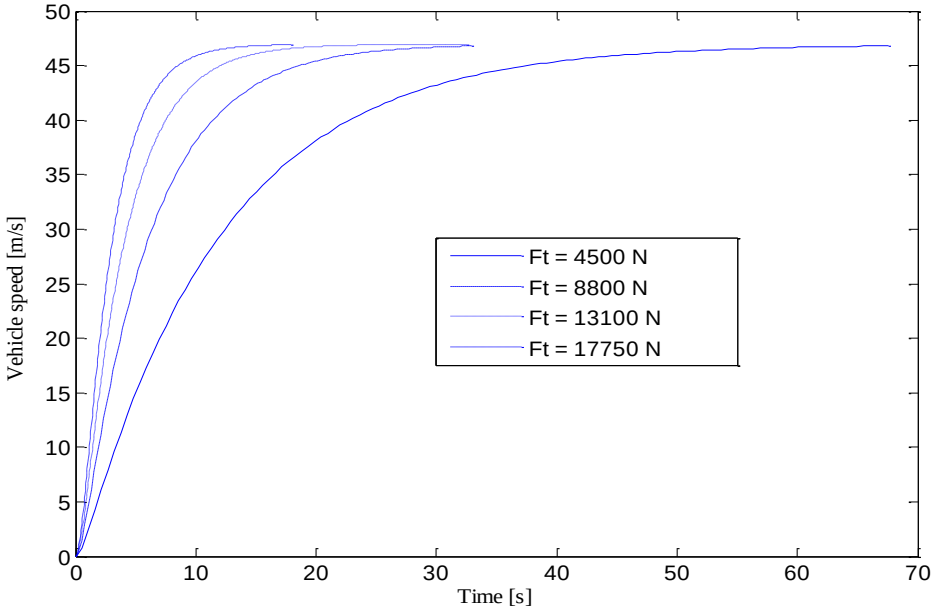

Figure 11: Vehicular Mobility Results of the Measured Road Segment at IRI 2.0 m/km

(c) IRI value of 3.0 m/km

Figure 12 show results for a length of 1000 m also. The simulation response was made for a vehicle run at a speed of 47 m/s on the road roughness. The time taken to cover the

distance at a tractive force of 4500 N by applying force of 50 N on accelerator pedal was 105.0 seconds. The time taken to cover the tractive forces of 8800 N on accelerator pedal of 100 N, 13100 N on accelerator pedal of 150 N and 17750 N on accelerator pedal of 200 N was 52.0 seconds, 36.5 seconds and 26.0 seconds respectively.

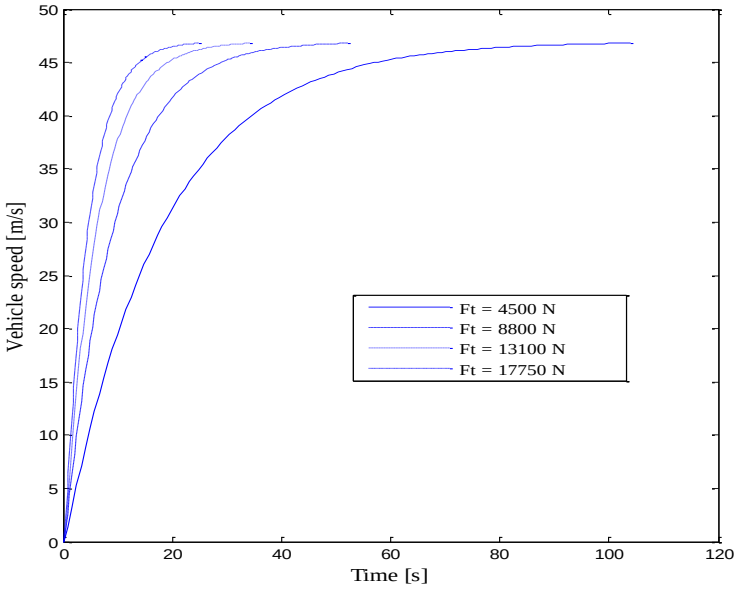

Figure 12: Mobility results of the measured segment at IRI 3.0 m/km

CONCLUSIONS

This study developed a mathematical model to analyze how internal factors influence road vehicle mobility, specifically considering the internal factors of tractive and pedal force. The findings reveal a clear relationship between road surface quality (roughness) and vehicle mobility, where vehicle mobility is significantly affected by the roughness of the road surface. Increased road roughness results in longer travel times and lower fuel efficiency. Increased tractive force reduces travel time across different road roughness levels. Higher pedal forces further reduce travel times, especially on smoother road segments, where times decrease depending on the tractive force. This study highlights the importance of road surface quality and vehicle operational parameters in optimizing vehicle mobility and efficiency. These outcomes emphasize the importance of maintaining road quality to enhance vehicle performance, reduce travel time, and improve fuel efficiency, ultimately contributing to safer and more comfortable driving conditions. The insights gained from this research can inform road maintenance practices and vehicle operation strategies, aiming to optimize mobility and minimize the adverse effects of road roughness on vehicle performance.

RECOMMENDATION

To ensure optimal vehicular mobility and road safety, it is essential to prioritize regular road surface maintenance. Aim to keep the International Roughness Index (IRI) value below 3.0 m/km. This proactive approach will mitigate the negative impacts of road roughness on vehicular performance and the overall driving experience. The model developed in this study offers a robust framework for analyzing the interactions between road surface conditions and vehicular mobility performance. Extending and refining this model to explore additional factors influencing vehicular dynamics can serve as a foundation for the continued development of more advanced vehicular mobility models, potentially leading to

significant improvements in road design, maintenance strategies, and vehicle performance.

NOMENCLATURE

A	front area	m^2
F	force	N
k	spring constant	N/m
M	mass	kg
n	engine sped	rpm
R	wheel radius	m
v	vehicle speed	m/s
x	rack displacement	mm
y	pedal displacement	mm
$\boldsymbol{\tau}$	time constant	sec
GREEK SYMBOLS		
K	Aerodynamic drag	
$\boldsymbol{\beta}$	number of driving wheel	
$\boldsymbol{\rho}$	density	$\boldsymbol{kg/m^3}$
$\boldsymbol{\omega}$	angular speed	rad/s
SUBSCRIPTS		
a	air	
d	damper	
e	engine	
n	constant	
o	constant drag	
r	gear box ratio	
s	spring	
t	traction	
v	vehicle	
w	wheel	
y	accelerator pedal	
ABBREVIATIONS		
G(s)	Transfer function	
IRI	International Roughness Index	
ISO	International Standard Organization	
MATLAB	MATrix LABoratory	
rpm	Revolution per minutes	

REFERENCES

Abera, Y. A. (2024). Sustainable building materials: A comprehensive study on eco-friendly alternatives for construction. *Composites and Advanced Materials,* **33,** 26349833241255957.

Abolore, R. S., Jaiswal, S. and Jaiswal, A. K. (2023). Green and sustainable pretreatment methods for cellulose extraction from lignocellulosic biomass and its applications: a review. *Carbohydrate Polymer Technologies and Applications***,** 100396.

Agwa, M., Youssef, S. M., Ali-Eldin, S. S. and Megahed, M. (2022). Integrated vacuum assisted resin infusion and resin transfer molding technique for manufacturing of nano-filled glass fiber reinforced epoxy composite. *Journal of Industrial Textiles,* **51,** 5113S-5144S.

Ahmad, J. and Zhou, Z. (2022). Mechanical properties of natural as well as synthetic fiber reinforced concrete: a

review. *Construction and Building Materials,* **333,** 127353.

Alam, A. M., Mina, M., Beg, M., Mamun, A., Bledzki, A. and Shubhra, Q. (2014). Thermo-mechanical and morphological properties of short natural fiber reinforced poly (lactic acid) biocomposite: Effect of fiber treatment. *Fibers and Polymers,* **15,** 1303-1309.

Elfaleh, I., Abbassi, F., Habibi, M., Ahmad, F., Guedri, M., Nasri, M. and Garnier, C. (2023). A comprehensive review of natural fibers and their composites: an eco-friendly alternative to conventional materials. *Results in Engineering***,** 101271.

Erturk-Avunduk, A. T., Cengiz-Yanardag, E. and Karakaya, I. (2022). The effect of bleaching applications on stained bulk-fill resin composites. *BMC Oral Health,* 22**,** 392.

Feng, Y., Hao, H., Lu, H., Chow, C. L. andLau, D. (2024). Exploring the development and applications of sustainable natural fiber composites: A review from a nanoscale perspective. *Composites Part B: Engineering***,** 111369.

Hadi, A.E., Siregar, J.P., Cionita, T., Norlaila, M.B., Badari, M.A.M., Irawan, A.P., Jaafar, J., Rihayat, T., Junid, R. and Fitriyana, D.F., 2022. Potentiality of utilizing woven pineapple leaf fibre for polymer composites. *Polymers*, *14*(13), p.2744.

Ho, M.-P., Wang, H., Lee, J.-H., Ho, C.-K., Lau, K.-T., Leng, J. andHui, D. (2012). Critical factors on manufacturing processes of natural fibre composites. *Composites Part B: Engineering,* 43**,** 3549-3562.

Hosseini, S. B., Gaff, M., Li, H. and Hui, D. (2023). Effect of fiber treatment on physical and mechanical properties of natural fiber-reinforced composites: A review. *Reviews on Advanced Materials Science,* **62,** 20230131.

Hoque, M.B., Mollah, M.Z.I., Faruque, M.R.I., Hannan, M.A. and Khan, R.A., 2021. Review on the mechanical properties of pineapple leaf fiber (PALF) reinforced epoxy resin based composites. *Polymer*, ***14***(15), pp.16-17

Ismail, S. O., Akpan, E. and Dhakal, H. N. (2022). Review on natural plant fibres and their hybrid composites for structural applications: Recent trends and future perspectives. *Composites Part C: Open Access*, **9,** 100322.

Jang, Y., Kim, J.H., Lee, D., Chon, J.S., Lee, S. and Kwon, D.J., 2024. Comprehensive analysis of the effect of braiding angle on the wettability and mechanical properties of 3D braided carbon fiber fabric-reinforced composites. *Materials Today Communications*, ***41***, p.110798.

Kamarudin, S. H., Mohd Basri, M. S., Rayung, M., Abu, F., Ahmad, S. B., Norizan, M. N., Osman, S., Sarifuddin, N., Desa, M. S. Z. M. andAbdullah, U. H. (2022). A review on natural fiber reinforced polymer composites (NFRPC) for sustainable industrial applications. *Polymers,* **14,** 3698.

Leão, A., Cherian, B., Narine, S., Souza, S., Sain, M. and Thomas, S. (2015). The use of pineapple leaf fibers (PALFs) as reinforcements in composites. *Biofiber reinforcements in composite materials***,** 211-235.

Lin, C., Kanstad, T., Jacobsen, S. and Ji, G., 2023. Bonding property between fiber and cementitious matrix: A critical review. *Construction and Building Materials*, ***378***, p.131169.

Mahajan, A., Binaz, V., Singh, I. andArora, N. (2022). Selection of natural fiber for sustainable composites using hybrid multi criteria decision making techniques. *Composites Part C: Open Access*, **7,** 100224.

Maiti, S., Islam, M. R., Uddin, M. A., Afroj, S., Eichhorn, S. J. andKarim, N. (2022). Sustainable fiber-reinforced composites: a Review. *Advanced Sustainable Systems,* **6,** 2200258.

Mohammad, F. (2014). Emerging green technologies and environment friendly products for sustainable textiles. *Roadmap to Sustainable Textiles and Clothing: Environmental and Social Aspects of Textiles and Clothing Supply Chain***,** 63-82.

Mohamed, R., Hapizi, N., Norizan, M.N. and Khairunnisa, N., 2021. Pineapple leaf fibers as a reinforcement of

biocomposites-an overview. *Polimery*, ***66***.

Nagaraja, S., Anand, P. B. andAmmarullah, M. I. (2024). Synergistic advances in natural fibre composites: a comprehensive review of the eco-friendly bio-composite development, its characterization and diverse applications. *RSC advances*, **14,** 17594-17611.

Neto, A. R. S., Araujo, M. A., Souza, F. V., Mattoso, L. H. andMarconcini, J. M. (2013). Characterization and comparative evaluation of thermal, structural, chemical, mechanical and morphological properties of six pineapple leaf fiber varieties for use in composites. *Industrial Crops and Products*, **43,** 529-537.

Prasad, V., Alliyankal Vijayakumar, A., Jose, T. andGeorge, S. C. (2024). A comprehensive review of sustainability in natural-fiber-reinforced polymers. *Sustainability*, **16,** 1223.

Rayung, M., Ibrahim, N. A., Zainuddin, N., Saad, W. Z., Razak, N. I. A. andChieng, B. W. (2014). The effect of fiber bleaching treatment on the properties of poly (lactic acid)/oil palm empty fruit bunch fiber composites. *International journal of molecular sciences*, **15,** 14728-14742.

Sanjay, M., Arpitha, G., Naik, L. L., Gopalakrishna, K. andYogesha, B. (2016). Applications of natural fibers and its composites: an overview. *Natural resources*, **7,** 108-114.

Santulli, C., Palanisamy, S. and Kalimuthu, M., 2022. Pineapple fibers, their composites and applications. In *Plant Fibers, their Composites, and Applications* (pp. 323-346). Woodhead Publishing.

Sawpan, M. A., Pickering, K. L. andFernyhough, A. (2012). Flexural properties of hemp fibre reinforced polylactide and unsaturated polyester composites. *Composites Part A: Applied Science and Manufacturing*, **43,** 519-526.

Sayam, A., Rahman, A. M., Rahman, M. S., Smriti, S. A., Ahmed, F., Rabbi, M. F., Hossain, M. andFaruque, M. O. (2022). A review on carbon fiber-reinforced hierarchical composites: mechanical performance, manufacturing process, structural applications and allied challenges. *Carbon Letters*, **32,** 1173-1205.

Sayem, A. S. M., Haider, J. andSayeed, M. A. (2020). Development and characterisation of multi-layered jute fabric-reinforced HDPE composites. *Journal of Composite Materials*, **54,** 1831-1845.

Sethupathi, M., Khumalo, M. V., Skosana, S. J. andMuniyasamy, S. (2024). Recent Developments of Pineapple Leaf Fiber (PALF) Utilization in the Polymer Composites—A Review. *Separations*, **11,** 245.

Shen, R., Liu, T., Liu, H., Zou, X., Gong, Y. andGuo, H. (2024). An Enhanced Vacuum-Assisted Resin Transfer Molding Process and Its Pressure Effect on Resin Infusion Behavior and Composite Material Performance. *Polymers*, **16,** 1386.

Thyavihalli Girijappa, Y. G., Mavinkere Rangappa, S., Parameswaranpillai, J. andSiengchin, S. (2019). Natural fibers as sustainable and renewable resource for development of eco-friendly composites: a comprehensive review. *Frontiers in materials*, **6,** 226.

Wasik, T., 2005. Effect of fiber volume fraction on fracture mechanics in continuously reinforced fiber composite materials.

Wulandari, A. P., Awis, V. P. D., Budiono, R., Kusmoro, J., Hidayat, S. S., Masruchin, N., Lubis, M. a. R., Fatriasari, W. andRachmawati, U. (2023). Tensile Strength Improvements of Ramie Fiber Threads through Combination of Citric Acid and Sodium Hypophosphite Cross-Linking. *Materials*, **16,** 4758.

Zabihi, O., Ahmadi, M., Nikafshar, S., Preyeswary, K. C. andNaebe, M. (2018). A technical review on epoxy-clay nanocomposites: Structure, properties, and their applications in fiber reinforced composites. *Composites part b: engineering*, **135,** 1-24.